

# Molecular signatures of disease brain endothelia provide new sites for CNS-directed enzyme therapy

Yong Hong Chen<sup>1</sup>, Michael Chang<sup>2</sup> & Beverly L Davidson<sup>1-3</sup>

**The brain vasculature forms an immense network such that most neural cells are in contact with a microvessel. Here we tested the hypothesis that endothelia lining these vessels can be harnessed to create a cellular reservoir of enzyme replacement therapy to diseased brain. As a model system, we used mice with central nervous system (CNS) deficits due to lysosomal storage disease (LSD mice). The basic premise of this work is that recombinant enzyme expressed in, and secreted from, the vascular endothelia will be endocytosed by underlying neurons and glia, decreasing neuropathology. We screened a phage library *in vivo* by panning to identify peptides that bound the vascular endothelia in diseased and wild-type mice. Epitopes binding diseased brain were distinct from those panned from normal brain. Moreover, different epitopes were identified in two distinct LSD disease models, implying a unique vascular signature imparted by the disease state. Presentation of these epitopes on the capsid of adeno-associated virus (AAV) expanded the biodistribution of intravenously injected AAV from predominantly liver to include the CNS. Peripheral injection of the epitope-modified AAVs expressing the enzymes lacking in LSD mice reconstituted enzyme activity throughout the brain and improved disease phenotypes in two distinct disease models.**

The vasculature of the mammalian CNS provides a potential site for delivery of secreted proteins to the brain, as endothelial cells lining those vessels are in close apposition to most underlying cells. Engineering brain endothelial cells to secrete a protein of interest, however, is problematic, because no mechanism has been shown to functionally modify brain endothelia *in situ*. As a first step to approach this problem, we injected a phage-display library intravenously into mice, similarly to previous reports<sup>1</sup>, and subsequently isolated the brain along with the bound phage. We then amplified and purified the isolated phage and injected it again (referred to as phage panning). Unlike previous work, which was done in normal brain<sup>1</sup>, we also panned in diseased mice. After five rounds of panning in  $\beta$ -glucuronidase-deficient mice, a model of the LSD mucopolysaccharidosis type VII (MPS VII), or their normal littermates, DNA sequencing of the recovered phage revealed enrichment of peptide motifs from the initial phage library (Fig. 1a,b). Notably, the motifs enriched in wild-type

mice were distinct from those in MPS VII mice, suggesting a vascular remodeling process in the diseased mice (Fig. 1a,b). Also, the motifs we identified in wild-type mice were different than the epitope found previously after panning (three rounds) in normal rats<sup>1</sup>.

In wild-type mouse brains, we identified the peptide motifs PXXPS, SPXXP, TLH and QSXY, where 'X' is any amino acid (Fig. 1a). In panning MPS VII mouse brain, the motifs LXSS, PFXG and SIXA were identified (Fig. 1b). Intravenous injection of selected, purified phages into naive mice confirmed significantly improved homing to brain relative to phage without peptide inserts, or phage representative of the unselected library (Fig. 1c,d). For wildtype mice (Fig. 1c), 13 of 15 epitopes were significantly enriched in brain relative to mice injected with the unselected library (groups 1–3,  $P < 0.05$ , Dunnett's *post hoc*). For MPS VII mice (Fig. 1d), 9 of 11 epitopes were significantly enriched in brain relative to mice injected with the unselected library (for all but GSIWAPA and SIAASFS,  $P < 0.05$ , Dunnett's *post hoc*).

To test the utility of the epitopes for brain endothelial targeting, we inserted sequences encoding them into loop IV of the AAV2 capsid at site 587 (ref. 2) (Supplementary Methods). AAVs generated by modifications at this site include AAV-linker (containing a linker sequence), AAV-TLH (containing the GWTLHNK epitope), AAV-PPS (epitope DSPAHPS), AAV-PFG (epitope WPFYGTGTP) and AAV-LSS (epitope LPSSLQK) (Supplementary Fig. 1). AAV-WT (no insert) and AAV-RGD (containing RGD epitope) served as additional controls. Four weeks after tail vein injections of AAV-WT, AAV-linker, AAV-RGD, AAV-PPS and AAV-TLH (into wild-type mice) or AAV-WT, AAV-PFG and AAV-LSS (into MPS VII mice), we assessed viral genomes in tissues. In wild-type mice, AAV-PPS was enriched in brain by several orders of magnitude (Fig. 2a). AAV-TLH had similarly improved brain targeting (Fig. 2a). In MPS VII mice, AAV-PFG homing was 35-fold higher in brain relative to liver, and had markedly improved brain tropism relative to AAV-WT (Fig. 2b). AAV-LSS was also significantly enriched over AAV-WT in MPS VII mouse brain, but, similar to AAV-TLH, liver transduction was nearly equivalent (Fig. 2b and Supplementary Tables 1 and 2).

We confirmed the extended tropism of AAV-PPS and AAV-PFG to include brain using AAVs expressing the reporter protein eGFP (AAV-PPS.eGFP) or  $\beta$ -glucuronidase (AAV-PFG. $\beta$ gluc). AAV-PPS.eGFP transduced brain microvessels in wild-type mice after peripheral injection (data not shown). We used an *in situ* enzyme

<sup>1</sup>Departments of Internal Medicine, <sup>2</sup>Molecular Physiology & Biophysics and <sup>3</sup>Neurology, University of Iowa, Iowa City, Iowa, USA. Correspondence should be addressed to B.L.D. (beverly-davidson@uiowa.edu).

Received 28 October 2008; accepted 12 August 2009; published online 13 September 2009; doi:10.1038/nm.2025

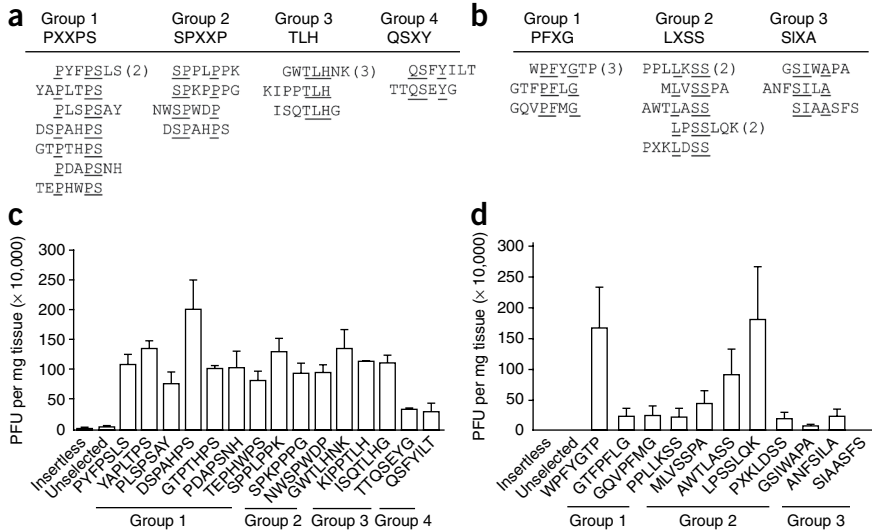


**Figure 1** *In vivo* phage display panning to identify peptide motifs with high affinity for cerebral vasculature. (a,b) Phage peptide sequences recovered after panning fall into four distinct motif groups for wild-type mice (a) and three motif groups for MPS VII mice (b). (c,d) Phage titers recovered from the cerebral vasculature of heterozygous (c) and MPS VII (d) mice after purified selected phage were individually injected via tail vein into naive mice ( $n = 3$  mice per phage). Data are presented as means  $\pm$  s.e.m.

activity stain to assess  $\beta$ -glucuronidase activity after peripheral injection of AAV-PFG. $\beta$ gluc. Heterozygous mice (Fig. 2c) and wild-type mice (data not shown) showed limited endogenous activity in brain using this assay and wild-type mice. Notably, AAV-PFG. $\beta$ gluc injection into MPS VII mice revealed overexpression of  $\beta$ -glucuronidase along large and small diameter vessels throughout the brain, in contrast to AAV-PFG. $\beta$ gluc-injected heterozygous mice (Fig. 2c). As a result, enzyme activity was elevated in cortex and brainstem (Supplementary Fig. 2). Confocal microscopy of sections immunostained with antibody to NeuN to detect neurons and antibody to  $\beta$ -glucuronidase showed colocalization of enzyme with NeuN in the underlying neuropil (Fig. 2d). Similar to AAV-WT, AAVs displaying epitopes panned from wild-type mice (AAV-TLH. $\beta$ gluc and AAV-PPS. $\beta$ gluc) did not transduce MPS VII mouse brain (data

not shown). Thus, the phage epitopes retained their specificity in the context of the AAVs. The region used for epitope insertion is important for AAV binding to its major receptor, heparan sulfate proteoglycan (HSPG), and insertion of peptides at this site often alters HSPG binding without compromising virus viability<sup>1,3,4</sup>. Our data are consistent with these findings; our modified capsid proteins packaged AAV vector genomes to yield titers comparable to those of wild-type virus (Supplementary Fig. 1), and the AAVs had reduced HSPG binding (Supplementary Fig. 3). We next tested the hypothesis that brain microvasculature endothelia can secrete recombinant enzymes sufficient to correct CNS deficits in the MPS VII mice model. The  $\beta$ -glucuronidase-deficient mouse used in our study shows hallmarks of MPS VII disease, including lysosomal storage and neurological dysfunction, and is a proven model for investigating new therapies for lysosomal storage disorders<sup>5</sup>. We injected AAV-PFG or AAV-WT expressing  $\beta$ -glucuronidase via tail vein into MPS VII mice at 6 weeks of age, as disease phenotypes, including lysosomal storage deposits, are apparent at this time. Four weeks later, we evaluated lysosomal storage and cellular distension in the brain. MPS VII mice treated with AAV-PFG. $\beta$ gluc exhibited reduced levels of lysosomal storage relative to mice receiving AAV-WT. $\beta$ gluc. We noted correction in the olfactory bulb, cerebral cortex, hippocampus, striatum and cerebellum (Fig. 3a). AAV-PFG. $\beta$ gluc, but not AAV-WT. $\beta$ gluc, significantly lowered the numbers of cells laden with storage vacuoles (Fig. 3b,  $P < 0.001$ ). Moreover, cellular dysmorphology improved after AAV-PFG. $\beta$ -gluc treatment, in contrast to control-treated mice (Fig. 3a). The correction of pathology in multiple cell types, along with colocalization of enzyme in neurons, suggests that  $\beta$ -glucuronidase was secreted basolaterally by endothelial cells and subsequently

© 2009 Nature America, Inc. All rights reserved.

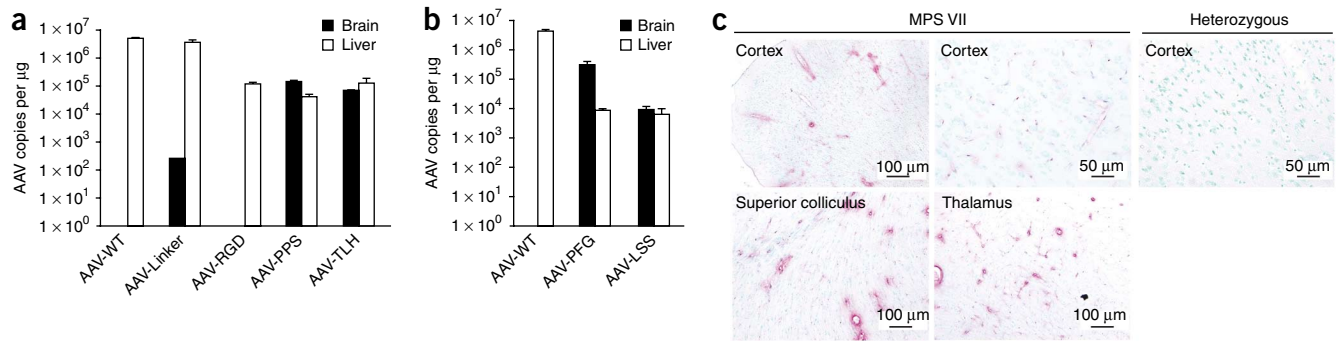


**Figure 2** Peptide epitopes expand the tropism of AAV2. (a,b) Viral genomes in brain and liver of wild-type (a) and MPS VII (b) mice, as quantified by quantitative PCR, after peripheral injection of indicated AAVs. Data are means  $\pm$  s.e.m.  $n = 3$  mice per group. (a) AAV-PPS and AAV-TLH were significantly enriched in brain versus AAV-WT ( $P < 0.001$ , Student's  $t$  test). (b) AAV-PFG and AAV-LSS were significantly enriched in brain versus AAV-WT ( $P < 0.001$ , Student's  $t$  test). (c) Representative sections, stained for  $\beta$ -glucuronidase activity *in situ* (red precipitate), show enzyme activity in MPS VII mice brain after injection with AAV-PFG. $\beta$ gluc (left and middle images). Top right image depicts the extent of staining in heterozygous mouse brain injected peripherally with AAV-PFG. $\beta$ gluc.  $n = 6$ –8 mice per group. (d) Representative confocal photomicrograph of brain cortex harvested from a MPS VII mouse injected by tail vein with AAV-PFG. $\beta$ gluc and immunostained with antibodies to  $\beta$ -glucuronidase (red) and the neuronal marker NeuN (green). Vascular (asterisk) and neuronal (arrows)  $\beta$ -glucuronidase-positive cells are indicated ( $n = 6$  mice).

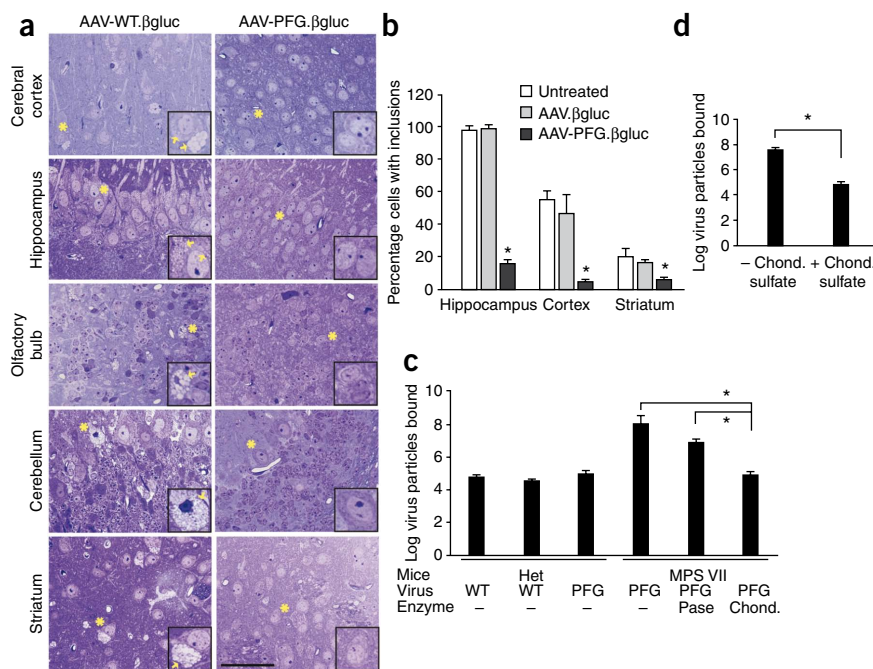


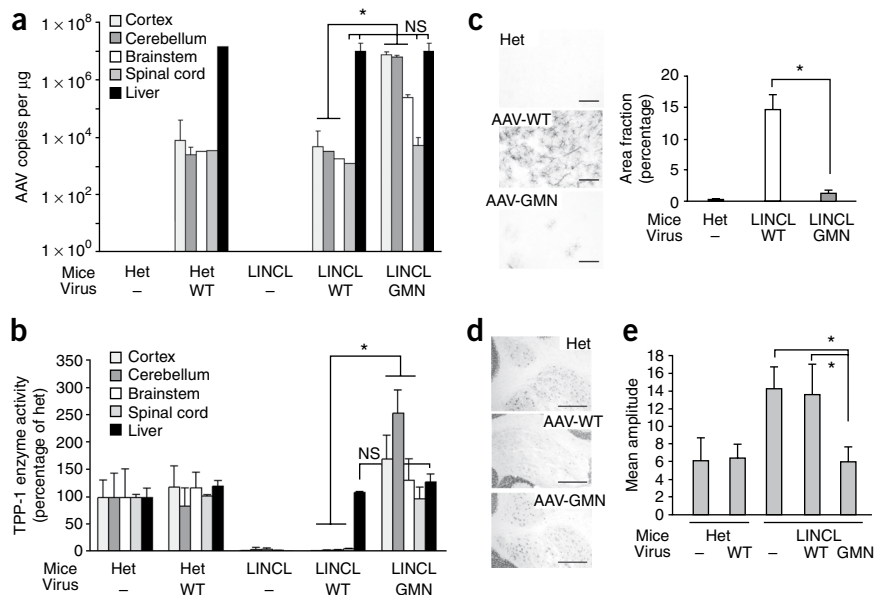
**Figure 3** Intravenous delivery of epitope-modified virus improves neuropathology in MPS VII mice. **(a)** Representative images from cerebral cortex, hippocampus, striatum, olfactory bulb and cerebellum of MPS VII mice, collected four weeks after tail vein injection with either AAV-WT.βgluc (left) or AAV-PFG.βgluc (right). Yellow asterisks denote regions magnified in insets (lower right, all images) for better visualization of storage vacuoles. Arrows in insets point to vacuoles.  $n = 4$  mice per group. Scale bar, 50  $\mu\text{m}$ . Inset magnification 5 $\times$ . **(b)** Quantification of vacuolar storage in various brain regions. Tail vein injection of AAV-PFG.βgluc but not AAV-WT.βgluc significantly reduced lysosomal storage vacuoles in hippocampus, cortex and striatum ( $*P < 0.001$ , Tukey's *post hoc*).  $n = 4$  mice per group. **(c)** Binding of AAV-PFG to MPS VII cerebral vasculature was decreased by chondroitinase treatment. Data show the levels of viral particles bound to purified microvessels from heterozygous (Het) or MPS VII mice brain after incubation with the indicated enzyme. Data are presented as means  $\pm$  s.e.m. ( $*P < 0.001$ , Dunnett's *post hoc*). Pase, PNGase; Chond, chondroitinase-ABC.  $n = 6$  mice per group. **(d)** Binding of AAV-PFG to purified brain vasculature from MPS VII mice in the presence or absence of chondroitin sulfate. Data are presented as means  $\pm$  s.e.m.  $*P < 0.01$ , Student's *t* test.  $n = 6$  mice per group.

cross-corrected adjacent neural cells. The correction of neuropathology in multiple structures throughout the rostral-caudal extent of the brain indicates broadly disseminated enzyme.

$\beta$ -glucuronidase catalyzes the degradation of glycosaminoglycans, including heparan sulfate and chondroitin sulfate. In the disease state, catabolism of these molecules is blocked and causes their accumulation. We hypothesized that epitope-modified AAV might interact with glycosaminoglycan-containing glycoproteins accumulating

on cell surfaces. Work with purified viral capsids indicated that endothelial cell binding of AAV-PFG is probably not mediated by heparan sulfate (**Supplementary Fig. 3**). To test a putative role for chondroitin sulfate, we measured the ability of AAV-PFG to bind brain vasculature from MPS VII mice in the presence or absence of the enzyme chondroitinase ABC. Enzymatic treatment of the vasculature from MPS VII mice abolished AAV-PFG binding (**Fig. 3c**). Furthermore, an excess of chondroitin sulfate was sufficient to

**Figure 4** An epitope panned from TPP1-deficient mice extends AAV tropism to brain and allows correction of CNS deficits. **(a)** Quantification of vector copy number in cortex, cerebellum, brainstem, spinal cord and liver after tail vein injection of AAV-GMN.TPP1 or AAV-WT.TPP1. Vector copy number for AAV-GMN.TPP1 was significantly higher than for AAV-WT.TPP1 in cortex, cerebellum and brainstem of LINCL-injected mice ( $*P < 0.005$ ). Vector copy number in spinal cord and liver were similar between AAV-GMN.TPP1 or AAV-WT.TPP1-injected LINCL mice ( $P = 0.12$  and  $0.61$ , respectively; Student's *t* test). NS, not significant.  $n = 3$  mice per group. **(b)** Enzyme activity in brain regions and liver after AAV-GMN.TPP1 or AAV-WT.TPP1 injection into mice. TPP1 activity was significantly higher in all brain regions and spinal cord of LINCL mice injected with AAV-GMN.TPP1 compared to AAV-WT.TPP1 ( $*P < 0.005$ ; Student's *t* test).  $n = 3$  mice per group. **(c)** Left, representative images showing GFAP immunoreactivity in the motor cortex of a heterozygous mouse (top), a LINCL mouse treated by tail vein with AAV-WT.TPP1 (middle) or a LINCL mouse treated by tail vein with AAV-GMN.TPP1 (bottom). Scale bars, 100  $\mu\text{m}$ . Right, quantification of GFAP staining ( $n = 3$  mice) shows significant reduction in glial activation in LINCL mice after treatment with AAV-GMN.TPP1 ( $*P < 0.001$ , Tukey's *post hoc*). **(d)** Representative photomicrographs of deep cerebellar nuclei in a heterozygous mouse (top), a LINCL mouse given a peripheral injection of AAV-WT.TPP1 (middle) or a LINCL mouse given a peripheral injection of AAV-GMN.TPP1 (bottom). Brain sections were immunostained with NeuN ( $n = 3$  mice per group). Scale bars, 500  $\mu\text{m}$ . **(e)** The effects of peripheral delivery of AAV-GMN.TPP1 versus AAV-WT.TPP1 on the tremor phenotype in LINCL mice. Tremor amplitude was significantly decreased in LINCL mice treated with AAV-GMN.TPP1 compared to AAV-WT.TPP1 ( $*P < 0.001$ , Dunnett's *post hoc*).  $n = 5$ –8 mice per group.



complete PFG-AAV binding (Fig. 3d). These data suggest that AAV-PFG binding to MPS VII mice brain vascular endothelia is due in part to accumulated chondroitin sulfate.

To investigate the broader utility of this approach, we repeated the *in vivo* panning in a mouse model of late infantile neuronal ceroid lipofuscinosis (LINCL mice). This model has mutations in *Tpp1*, lacks expression of the lysosomal enzyme tripeptidyl peptidase I (TPP-1) and recapitulates many pathological features of the human disease<sup>6,7</sup>. After five rounds of *in vivo* phage panning, a single dominant peptide emerged: GMNAFRA. Notably, the epitope identified from panning in LINCL mice was distinct from those identified in wild-type or MPS VII mice, supporting the concept of a disease-specific vascular remodeling process. As before, we produced an epitope-modified AAV expressing TPP-1 (AAV-GMN.TPP1). AAV-WT genomes were predominantly localized to liver after peripheral injection into LINCL mice or heterozygous littermates (Fig. 4a and Supplementary Fig. 4). In contrast, we found AAV-GMN.TPP1 viral genomes at roughly equivalent levels in liver, cerebral cortex and cerebellum after tail vein injection into LINCL mice (Fig. 4a).

We detected TPP-1 activity in liver (Fig. 4b) and other peripheral tissues (Supplementary Fig. 5) 6 weeks after delivery of AAV-WT.TPP1 into tail veins of mutant or heterozygous mice. There was no detectable expression in brain above background levels (Fig. 4b). AAV-GMN.TPP1, which by viral genome analyses reached brain after tail vein injection (Fig. 4a), normalized TPP-1 activity to the levels found in heterozygous mice in cerebral cortex, cerebellum, brainstem and spinal cord relative to AAV-WT.TPP1-injected LINCL mice (Fig. 4b). TPP-1 activity in the spinal cord was likely due to transduction elsewhere in the CNS, as the number of vector copies in the spinal cord was low relative to other brain regions. As with AAV-PFG.βgluc, AAV-GMN.TPP1 did not increase TPP-1 activity in brain when injected into heterozygous littermates (data not shown). Also, AAV-PFG.βgluc did not transduce LINCL brain (data not shown).

We next tested how peripheral delivery of AAV-GMN.TPP1 or AAV-WT.TPP1 to 8-week-old *Tpp1*<sup>-/-</sup> mice affected readouts of disease progression. Notable phenotypes in LINCL mice include progressive loss of the deep cerebellar nuclei, glial activation in the motor cortex, as evidenced by enhanced glial fibrillary acidic protein (GFAP) immunoreactivity, and a progressive resting tremor<sup>7</sup>. Although both AAV-WT.TPP1 and AAV-GMN.TPP1 reconstituted peripheral enzyme activity in LINCL mice (Supplementary Fig. 5), only AAV-GMN.TPP1 improved CNS pathology (Fig. 4c,d) and prevented the tremor phenotype (Fig. 4e). Together, these data show that transduction of the CNS vasculature can promote dissemination of a therapeutic enzyme into the mammalian brain.

Previous work has shown that organ-specific epitopes can be isolated after *in vivo* panning after intravenous injection of phage libraries<sup>1,2</sup>. However, our identification of various epitopes after phage display panning in brains from wild-type and disease mouse models implies molecular differences in the vascular bed, depending on disease state, that were previously unappreciated. In some instances, the epitopes panned from the brain expanded the tropism of the AAV to include the brain (PPS and TLH panned from WT mice, LSS panned from MPS VII mice and GMN panned from TPP-1-deficient mice). Or, the tropism was shifted from predominately liver targeting to

predominantly brain targeting (PFG panned from MPS VII mice). And, although AAV-GMN and AAV-WT allowed transduction of peripheral organs, only the former corrected the CNS manifestations of the disease. Our data demonstrate that peripheral delivery of modified AAVs to adult mice can ameliorate brain phenotypes in LSD models.

Because the epitopes emerging from the *in vivo* panning of the MPS VII brain bound in part to accumulated chondroitin sulfate, they may be generally applicable for retargeting drugs, enzymes or vectors for other types of neuronopathic MPS. Finally, the use of AAV libraries generated by inserting amino acid sequences into the viral capsid or by capsid shuffling<sup>3,8–10</sup> may provide another source for targeting brain endothelia. Such reagents will be generally useful for studying biological properties of this tissue *in situ* and how those properties are altered in disease states.

## METHODS

Methods and any associated references are available in the online version of the paper at <http://www.nature.com/naturemedicine/>.

*Note: Supplementary information is available on the Nature Medicine website.*

## ACKNOWLEDGMENTS

We thank G. Liu and J. Wilson for technical assistance and the Central Microscopy Research Facility at the University of Iowa. We thank C. Stein and P. Staber for reading of the manuscript. We thank W. Sly, St. Louis University, for goat antibody to β-glucuronidase. This work was supported by the US National Institutes of Health (grants HD33531, NS34568 and DK54759), the Batten Disease Research and Support Association and the Roy J. Carver Trust.

## AUTHOR CONTRIBUTIONS

Y.H.C. designed and performed the experiments and edited the paper, M.C. performed experiments and edited the paper, and B.L.D. developed the study, designed experiments and wrote the paper.

Published online at <http://www.nature.com/naturemedicine/>.

Reprints and permissions information is available online at <http://npg.nature.com/reprintsandpermissions/>.

1. Work, L.M. *et al.* Vascular bed-targeted *in vivo* gene delivery using tropism-modified adeno-associated viruses. *Mol. Ther.* **13**, 683–693 (2006).
2. Grifman, M. *et al.* Incorporation of tumor-targeting peptides into recombinant adeno-associated virus capsids. *Mol. Ther.* **3**, 964–975 (2001).
3. Müller, O.J. *et al.* Random peptide libraries displayed on adeno-associated virus to select for targeted gene therapy vectors. *Nat. Biotechnol.* **21**, 1040–1046 (2003).
4. Perabo, L. *et al.* Heparan sulfate proteoglycan binding properties of adeno-associated virus retargeting mutants and consequences for their *in vivo* tropism. *J. Virol.* **80**, 7265–7269 (2006).
5. Vogler, C. *et al.* A novel model of murine mucopolysaccharidosis type VII due to an intracisternal a particle element transposition into the β-glucuronidase gene: clinical and pathologic findings. *Pediatr. Res.* **49**, 342–348 (2001).
6. Sleat, D.E. *et al.* A mouse model of classical late-infantile neuronal ceroid lipofuscinosis based on targeted disruption of the CLN2 gene results in a loss of tripeptidyl-peptidase I activity and progressive neurodegeneration. *J. Neurosci.* **24**, 9117–9126 (2004).
7. Chang, M. *et al.* Intraventricular enzyme replacement improves disease phenotypes in a mouse model of late infantile neuronal ceroid lipofuscinosis. *Mol. Ther.* **16**, 649–656 (2008).
8. Maheshri, N., Koerber, J.T., Kaspar, B.K. & Schaffer, D.V. Directed evolution of adeno-associated virus yields enhanced gene delivery vectors. *Nat. Biotechnol.* **24**, 198–204 (2006).
9. Koerber, J.T., Maheshri, N., Kaspar, B.K. & Schaffer, D.V. Construction of diverse adeno-associated viral libraries for directed evolution of enhanced gene delivery vehicles. *Nat. Protoc.* **1**, 701–706 (2006).
10. Grimm, D. *et al.* *In vitro* and *in vivo* gene therapy vector evolution via multispecies interbreeding and retargeting of adeno-associated viruses. *J. Virol.* **82**, 5887–5911 (2008).

## ONLINE METHODS

**Experimental mice.** We obtained MPS VII carrier mice (B6.C-H-2<sup>bm1</sup>/ByBir-Gus<sup>m<sup>ps</sup></sup>/J) from the Jackson Laboratory, and we subsequently bred and maintained them at the University of Iowa animal facility. The LINCL mouse model has a *neo* insertion in intron 11 and has the Arg446His mutation in *Tpp1* (ref. 6). It is essentially a null mutant and, for brevity, is referred to as *Tpp1*<sup>-/-</sup>. All mouse maintenance conditions and experimental protocols were approved by the University of Iowa Animal Care and Use Committee.

**In vivo biopanning.** We injected MPS VII, LINCL or wild-type mice (6–8 weeks of age) with  $2 \times 10^{10}$  plaque-forming units (PFU) of phage from the Ph.D.7 phage display library (New England Biolabs) in 200  $\mu$ l DMEM (Invitrogen) through the tail vein. After 5 min, we anesthetized the mice and perfused them transcardially with DMEM. We extracted the brains and recovered and amplified the phages. We then purified, titered and re-injected the amplified phages in each of five consecutive rounds of panning. We kept the input phage at  $2 \times 10^{10}$  PFU per mice for each round. After the fifth round of panning, we sequenced DNA from randomly selected clones. To verify that the selected phages bound the brain vasculature, we amplified the selected phages from the fifth round of panning individually, purified them and injected  $2 \times 10^{10}$  PFU through the tail vein ( $n = 3$  per phage motif). After 5 min, we perfused the mice transcardially with DMEM, extracted their brains and recovered and titered the binding phage. We used a phage with no insert and the original unselected Ph.D.7 phage display library as controls.

**In situ enzyme activity assay for  $\beta$ -glucuronidase activity and morphological assays.** We anesthetized mice injected with AAVs ( $1.0 \times 10^{12}$  genome particles) and transcardially perfused them with ice-cold 2% paraformaldehyde 4 weeks after injection. We collected their brains, embedded them in optimal cutting temperature compound and sectioned them (16  $\mu$ m thick) on a cryostat. For  $\beta$ -glucuronidase activity staining, we assayed sections from mice ( $n = 6$ –8 per group, ten sections per mouse) using established methods<sup>11</sup>. For morphological assays, we transcardially perfused the mice ( $n = 4$  per group) with 2% paraformaldehyde and 2% glutaraldehyde in PBS, collected the brains and then postfixed in the same fixative at 4 °C overnight. We prepared and analyzed the tissues as previously described<sup>11</sup>. To quantify vacuolar storage, we counted 200 cells per region over three or four sections per mouse.

**TPP-1 activity assay.** We injected LINCL (6–8 weeks old) mice and heterozygous littermates ( $n = 3$  per group) intravenously with  $1.0 \times 10^{12}$  genome particles of wild-type AAV2 or epitope-modified AAV2 via the tail vein. Six weeks later, we transcardially perfused the mice with ice-cold normal saline and extracted tissues and homogenized for enzyme assay using established methods<sup>7</sup>.

**Quantification of tremor in TPP-1-deficient mice.** We injected *Tpp1*<sup>-/-</sup> (6–8 weeks) and age-matched *Tpp1*<sup>+/-</sup> mice ( $n = 5$ –8 per group) intravenously with  $1.0 \times 10^{12}$  genome particles of wild-type AAV2 or epitope-modified AAV2

via the tail vein. Six weeks later, we assessed mean tremor amplitudes with a tremor monitor (SD Instruments) using established methods<sup>7</sup>.

**Immunohistochemistry.** We anesthetized mice injected with AAVs ( $1.0 \times 10^{12}$  genome particles;  $n = 3$  per group) and transcardially perfused them with normal saline followed by 4% paraformaldehyde in normal saline. We then extracted their brains and postfixed them by standard methods. We analyzed sections (40  $\mu$ m thick) with a goat antibody to  $\beta$ -glucuronidase (a gift from W. Sly, St. Louis University, 1 in 200), mouse antibody to NeuN (Chemicon, MAB 377, 1 in 500), and rabbit antibody to GFAP (Dako, Z0334, 1 in 2,000). We then used biotinylated secondary antibody (Jackson ImmunoResearch, 1 in 200) or fluorescence-conjugated secondary antibody (Invitrogen, 1 in 500). Where appropriate, we developed slides with diaminobenzidine peroxidase substrate kit (Vector Laboratories).

**Analysis of adeno-associated virus binding.** We isolated mouse brain vasculature by centrifuging crude brain homogenate in 15% dextran and further purified it by running it through 105- $\mu$ m and 70- $\mu$ m meshes, as previously described<sup>12</sup>. We incubated 50  $\mu$ g of the brain vasculature separated by the 70- $\mu$ m mesh with PBS alone, PNGase (100 U per reaction) or chondroitinase ABC (2 U per reaction) at 37 °C for 1 h (Sigma-Aldrich). We stopped the reaction by adding cold PBS and washed it three times. We then incubated the treated vasculatures with virus ( $1.0 \times 10^{11}$ ) in 500  $\mu$ l PBS with 0.1% BSA at 4 °C for 1 h. After washing, we isolated the DNA and analyzed viral genomic particles by real-time PCR. For competitive binding of AAV-PFG to brain vasculature of MPS VII mice, we incubated 50  $\mu$ g of brain vasculature with AAV-PFG ( $1.0 \times 10^{11}$ ) in the presence or absence of 2 mg ml<sup>-1</sup> chondroitin sulfate at 4 °C for 1 h. We analyzed bound virus by real-time PCR.

**Statistical analyses.** We analyzed data by paired Student's *t* tests where appropriate. For **Figure 3b**, one-way ANOVA revealed significant group effects for vacuolar storage in hippocampus ( $F_{2,11} = 2129$ ;  $P < 0.0001$ ), cortex ( $F_{2,11} = 58.05$ ;  $P < 0.0001$ ) and striatum ( $F_{2,11} = 27.62$ ;  $P < 0.0001$ ). For **Figures 3c, 4c and 4e**, one-way ANOVA revealed significant group effects ( $F_{2,17} = 103.3$ ;  $P < 0.0001$ ), ( $F_{2,21} = 64.45$ ;  $P < 0.0001$ ) and ( $F_{2,32} = 19.27$ ;  $P < 0.0001$ ), respectively (StatView software; SAS Institute).

**Additional methods.** Detailed methodology is described in the **Supplementary Methods**.

- Liu, G., Martins, I., Wemmie, J., Chiorini, J. & Davidson, B. Functional correction of CNS phenotypes in a lysosomal storage disease model using adeno-associated virus type 4 vectors. *J. Neurosci.* **25**, 9321–9327 (2005).
- Song, L. & Pachter, J.S. Culture of murine brain microvascular endothelial cells that maintain expression and cytoskeletal association of tight junction-associated proteins. *In Vitro Cell. Dev. Biol. Anim.* **39**, 313–320 (2003).